Catena 228 (2023) 107119

Contents lists available at ScienceDirect

Catena

journal homepage: www.elsevier.com/locate/catena

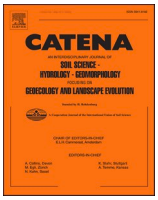

A middle Pleistocene to Holocene perspective on sediment sources for the Tengger Desert, China

Maotong Li [a], Junsheng Nie [a,*], Zaijun Li [a,*], Alex Pullen [b], Jordan T. Abell [c], Haobo Zhang [a], Cody A. McMechen [b], Baotian Pan [a]

[a] Key Laboratory of Western China's Environment Systems (Ministry of Education), College of Earth and Environmental Sciences, Lanzhou University, Lanzhou 730000, China
[b] Department of Environmental Engineering and Earth Sciences, Clemson University, Clemson, SC 29634, USA
[c] Department of Geosciences, University of Arizona, Tucson, AZ 85721, USA

ARTICLE INFO

Keywords:
Tengger Desert
Aridification
Qilian Mountains
Provenance
U-Pb geochronology

ABSTRACT

Dust plays a critical role in global biogeochemical and carbon cycles. The deserts of northern China have been important East Asian dust sources throughout the Quaternary. The Tengger Desert, one such major arid dust-producing region in northern China, is thought to have started resembling its current form during the middle to late Pleistocene. As such, understanding the nature of the Tengger Desert's formation and the associated import, storage, and export of sediments are consequential for the regional, and potentially global, climate. The U-Pb detrital zircon geochronology data reported here from both present-day and middle to late Pleistocene Tengger Desert sediments support derivation from the Shiyang River system sourced from the Qilian Mountains mixed with sediments eroded from local basement uplifts and Gobi Altay sources. This interpretation is different from the view that sediments of this age were primarily transported to the Tengger Desert from the arid East Asian continental interior upwind. We note that this analysis suggests a common provenance for Quaternary sediments in the Tengger, Badain Jaran, and Mu Us Deserts wherein these deserts received riverine-sourced sediments from the Qilian Mountains and northeastern Tibetan Plateau. This observation highlights the importance of precipitation at elevation along the present-day margin of the East Asian summer monsoon in driving sediment supply during the middle to late Quaternary desertification within the East Asian continental interior.

1. Introduction

Major geological events, like orogenesis, occurred throughout the Cenozoic, leading to remarkable changes in regional and global climates (An et al., 2001; Ravelo et al., 2004; Haug et al., 2005; Fedorov et al., 2006; Nie et al., 2014; Raymo et al., 2006; Craddock et al., 2010). Of these events, the desertification of the eastern Asian continental interior is one that had a profound impact on environmental conditions and climate at both regional and global levels. Recent estimates based on various modeling approaches suggest that approximately 180–580 Tg of dust is emitted from East Asia annually (Kok et al., 2021), which is subsequently deposited in regions downwind such as the North Pacific Ocean, North America, and Greenland (Uno et al., 2009; Újvári et al., 2022). Importantly, the lithogenic dust delivered to the North Pacific provides micronutrients like iron to autotrophic marine organisms which can ultimately impact the global carbon cycle (Martin, 1990; Tagliabue et al., 2017). Consequently, the timing and formation mechanisms of deserts have attracted the attention of geoscientists (e.g., Pullen et al., 2011; Sun et al., 2011; Stevens et al., 2013; Nie et al., 2015; Yang et al., 2015; Zheng et al., 2015; Rittner et al., 2016; Abell et al., 2020; Pastore et al., 2021; Garzanti et al., 2022; Zhao et al., 2022).

At least two important conditions are required to form and maintain sandy deserts: 1) a sufficient supply of sand particles where supply-in is equal to or greater than export out of the system; and 2) dry surface conditions lacking vegetation (Bullard and Livingstone, 2002). Winds, persistent or gusty, are also important for sediment transport and aerosol production within deserts (Kurosaki and Mikami, 2003; Kocurek and Ewing, 2005; Engelstaedter and Washington, 2007; McGee et al., 2010). Outward expansion and surface uplift of the Tibetan Plateau is widely held as the major forcing agent influencing the development of

* Corresponding authors.
E-mail addresses: jnie@lzu.edu.cn (J. Nie), zjli@lzu.edu.cn (Z. Li).

https://doi.org/10.1016/j.catena.2023.107119
Received 10 August 2022; Received in revised form 15 March 2023; Accepted 26 March 2023
Available online 13 April 2023

deserts in northern China during the Neogene (Guo et al., 2002; Ding et al., 2005). Uplift of the Tibetan Plateau is thought to have strengthened the atmospheric Siberian high which intensified the East Asian winter monsoon (An et al., 2001; Zhang et al., 2015), the breakdown of which is responsible for springtime dust transport through deserts and downwind to the Chinese Loess Plateau and the North Pacific Ocean (Roe, 2009). This process may have been amplified by enhanced meridional temperature gradients during global cooling since the late

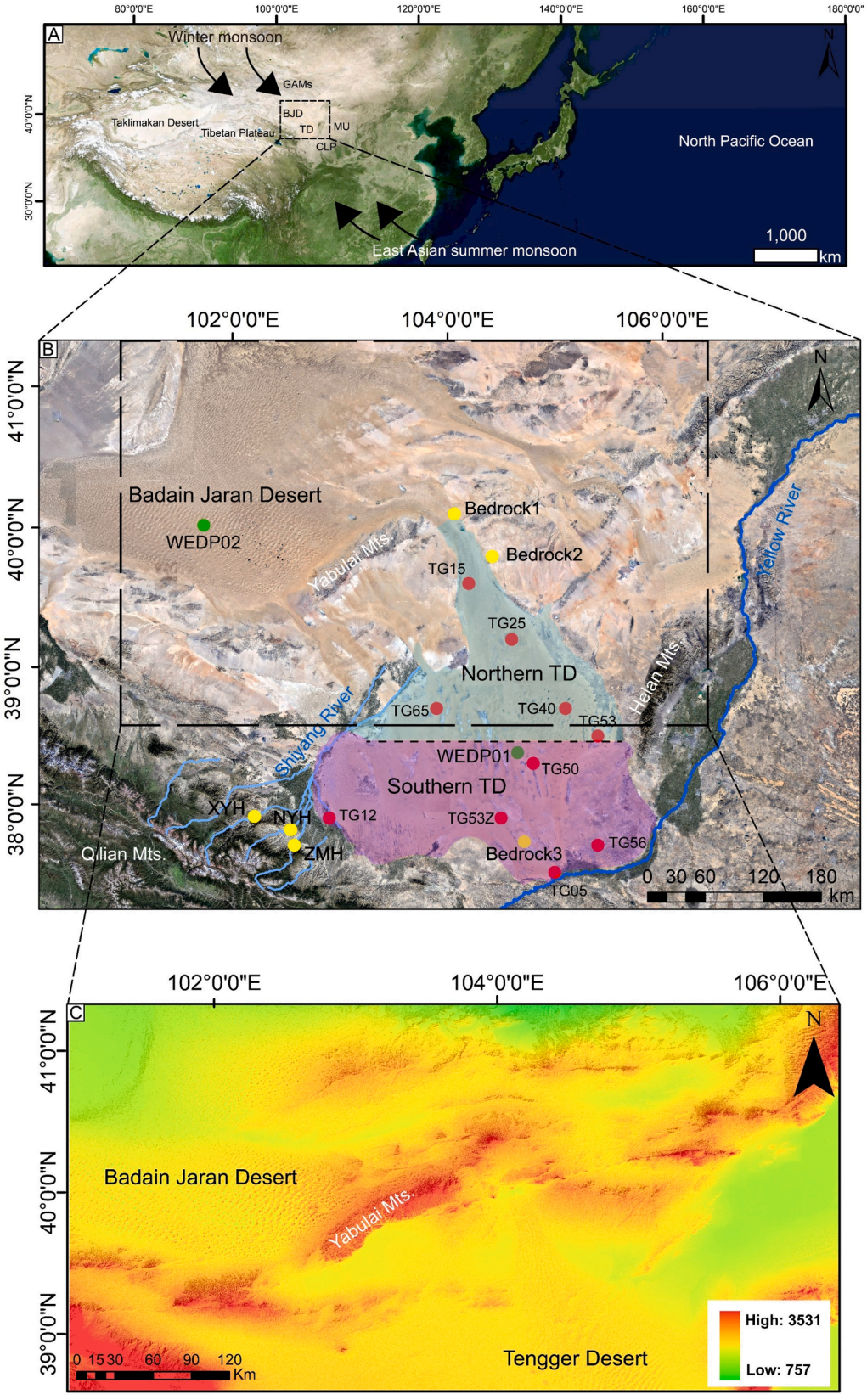

Fig. 1. (A) Map of central and eastern Asia and the North Pacific Ocean. (B) The Tengger Desert (TD) geographic location and detrital zircon sample sites. (C) Digital elevation map of the study area derived from NASA DEM (30 m). The dashed rectangles in (A) and (B) correspond to the areas of (B) and (C). Yellow and green dots indicate the locations of potential source samples and drill cores (WEDP01 and WEDP02), respectively. Red dots indicate the locations of the previously published sites within the TD (Zhang et al., 2016). BJD — Badain Jaran Desert, TD — Tengger Desert, MU — Mu Us Desert, CLP — Chinese Loess Plateau, GAMs — Gobi Altay Mountains. XYH, NYH, and ZMH— Three branch rivers of the Shiyang River.

Miocene (Herbert et al., 2016). Additionally, in this scenario, uplift enhanced exhumation, thus providing more unconsolidated sediments to basins, and enhanced aridity through orographic blocking (Guo et al., 2002; Sun and Liu, 2006; Heermance et al., 2018). Many lines of evidence, including low-temperature thermochronology, crustal deformation, and stable isotope records, support a phase of late Miocene uplift of the northeastern Tibetan Plateau (An et al., 2001; George et al., 2001; Fang et al., 2005; Bovet et al., 2009; Zheng et al., 2010; Hough et al., 2011; Duvall et al., 2013; Li et al., 2014a). This timing is consistent with the initiation of dust deposition on the central and eastern Chinese Loess Plateau, suggesting a direct causal relationship (Sun et al., 1998; Guo et al., 2001; Qiang et al., 2001; Song et al., 2001).

However, the desertification of the eastern Asian continental interior during the Neogene and Quaternary was protracted. The formation of the Taklimakan Desert in the Tarim Basin occurred in the early Miocene and early Pliocene in response to the retreat of the Paratethys sea, with the Mediterranean salinity crisis acting as an additional forcing agent (Sun and Liu, 2006; Zheng et al., 2015; Sun et al., 2017; Heermance et al., 2018). Liu et al. (2020) advocated for greater permanence of the Taklimakan Desert around 1 Ma, invoking global cooling across the Mid-Pleistocene Transition and enhanced glacial grinding to produce more detritus transported to the basin. Similarly, other eastern Asian deserts such as the Badain Jaran Desert and Tengger Desert (TD) are reported to have developed over the middle to late Quaternary (Li et al., 2014b; Wang et al., 2015), but the forcing mechanisms are less well constrained.

To *i*) better constrain desertification in the TD, *ii*) improve our understanding of sediment routing into the TD, and *iii*) compare TD sediment sourcing with proximal desert regions to assess export from the TD, we analyze the provenance of middle Pleistocene to Holocene sediments in the TD. Specifically, we present detrital zircon U-Pb geochronology data from three rivers draining to the TD, three local basements exposures, and samples from one sediment drill core (Fig. 1). Finally, we compare our new ages with published data from TD surface samples.

2. Geographical setting, sampling, and methods

The TD is the fourth largest desert in China by area. This arid region is separated from the Mu Us Desert by the Yellow River and the Helan Mountains on the southeast and the east, and from the Badain Jaran Desert by the Yabulai Mountains on the northwest (Fig. 1). The Qilian Mountains of the northeastern Tibetan Plateau bound the TD to the southwest (Fig. 1). Present-day precipitation in the Qilian Mountains is in the range 20–500 mm/year with a strong summer signal in the east from the East Asian summer monsoon (Li et al., 2015; Geng et al., 2017). This feeds the Shiyang River which coalesces from tributaries in the Qilian Mountains and presently terminates in the arid northwestern TD (Fig. 1B).

Continuous sandy eolian deposits appear in the stratigraphic record of the central TD at ~ 0.9 Ma (Li et al., 2014b; core WEDP01; Fig. 1). Pliocene–lower Pleistocene strata in the central TD indicate primarily alluvial, fluvial, and lacustrine depositional environments (Li et al., 2014b). Li et al. (2018) noted the onset of uninterrupted dust deposition at ~ 2.6 Ma in the TD, but associated desert formation—not defined, but inferred to be a transition away from alluvial-fluvial-lacustrine depositional environments—with the onset of continuous eolian activity at ~ 0.9 Ma.

We report detrital zircon U-Pb ages for two drill core (WEDP01) samples in the TD (Fig. 1 and Table 1). Core WEDP01 (38°22′42″ N, 104°39′17″ E) is located in the central TD, from which we collected two sand samples (H70 and H200), with depositional ages of ~ 0.05 and ~ 0.87 Ma, respectively (Li et al., 2014b). The age model of the Tengger cores has been established by Li et al. (2014b), which was based on paleomagnetic dating in combination with electron spin resonance dating. We estimated the depositional ages of selected samples by linear interpolation between geomagnetic reversals (Li et al., 2014b). Bedrock samples 1 and 2 are igneous rocks and bedrock sample 3 is sandstone.

Table 1
Location, sample number, and sample type from the Tengger Desert in this study.

Sample Name	n	Location		Sample Type
		Latitude (°N)	Longitude (°E)	
Bedrock1	426	40°05′51.60″	104°03′56.37″	Local bedrock
Bedrock2	389	39°47′35.29″	104°25′03.59″	Local bedrock
Bedrock3	1119	37°43′33,74″	104°42′59.37″	Local bedrock
XYH	979	37°54′44.06″	102°12′15.64″	Branch river sediment of the Shiyang River
ZMH	877	37°42′2.34″	102°34′32.71″	Branch river sediment of the Shiyang River
NYH	1003	37°48′50.96″	102°32′32.68″	Branch river sediment of the Shiyang River
H70	736	38°22′42″	104°39′17″	WEDP01 drill core
H200	831	38°22′42″	104°39′17″	WEDP01 drill core

The river samples were taken from floodplains. To avoid the interference of human activities, the top 3–5 cm of surface sediments were removed when sampling the floodplains. We also compare these detrital zircon U-Pb geochronology data with ten active eolian sand dunes across the TD previously published by Zhang et al. (2016).

The detrital zircon U-Pb ages were measured at the Arizona LaserChron Center at the University of Arizona following the analytical methods of Sundell et al. (2021). Measurements were completed using a Teledyne Photon Machines G2 excimer ArF laser ablation system coupled to a Nu Plasma HR multi-collector (MC) inductively-coupled-plasma mass spectrometer (ICP-MS), at a rate of 600 analyses/hour (6 s per analysis). The laser energy was set at a 7 mJ output at 7 Hz using a constant energy mode. The analyte aerosol was carried to the MC-ICP-MS in a He carrier gas and mixed with Ar before reaching the plasma. Mounts were cleaned in a 1% HCl – 1% HNO_3 solution before ablation. Before each analysis, a pre-ablation cleaning pass of three pulses at 50 μm was made with the laser to remove surface contamination followed by the 30 μm analysis ablation. Faraday collectors were used to measure ^{238}U, ^{232}Th, ^{208}Pb, ^{207}Pb, and ^{206}Pb, whereas mass-202 (i.e., $^{202}Hg + Pb$) and ^{204}Pb were measured in ion multiplying detectors. The uncertainties of all samples are reported at the 1σ level (reflecting analytical uncertainty). We use the $^{206}Pb/^{238}U$ ages for younger than 1000 Ma and the $^{207}Pb/^{206}Pb$ ages for older than 1000 Ma. For ages younger than 1000 Ma, we defined the discordance as (($^{207}Pb/^{235}U$-$^{206}Pb/^{238}U$)/$^{207}Pb/^{235}U$*100); for ages older than 1000 Ma, we defined the discordance as (($^{207}Pb/^{206}Pb$-$^{206}Pb/^{238}U$)/$^{207}Pb/^{206}Pb$*100). Analyses with > 15% discordance and with > 10% reverse discordance were not included for interpretation. The results were plotted using the multidimensional scaling (MDS) statistical approach (Vermeesch, 2013; Saylor et al., 2018) and the detrital zircon DZ-Mix model (Sundell and Saylor, 2017).

3. Results

The two drill core samples show four groups of ages: 2800–1600 Ma, 1200–800 Ma, 500–400 Ma, and 300–200 Ma, of which the 300–200 Ma age range yielded the highest probability (Fig. 2D and E). This pattern is different from the three river samples which show a similar pattern in which the 500–400 Ma ages have the highest probability (Fig. 2F–H). Additionally, the 2800–1600 Ma and the 1200–800 Ma ages are less abundant in the river samples than in the drill core samples (Fig. 2D–H). Bedrock 1 and 2 only have ages within the 310–250 Ma range; by contrast, Bedrock 3 only has ages in the 2800–1600 Ma range without ages in the other three age ranges being observed (Fig. 2I–K).

The MDS plot shows that published U-Pb data for the TD surface samples (Zhang et al., 2016) cluster geographically into a southern and a northern region (Fig. 3). The southern TD is composed of samples TG12, TG56, TG53Z, and TG50 (Fig. 1). These samples plot close to the Shiyang

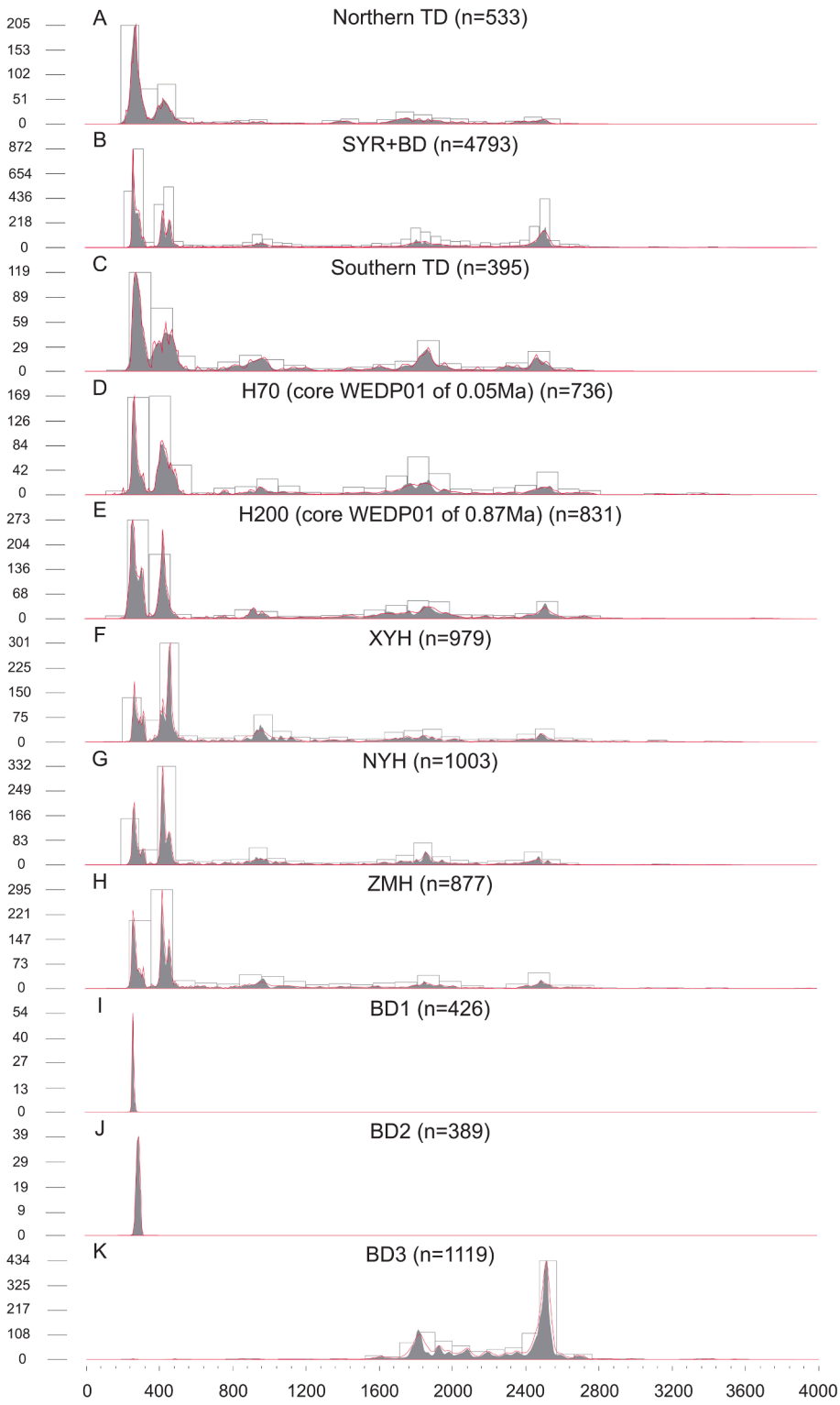

Fig. 2. Zircon U-Pb ages from the Tengger Desert (TD) deposits and potential sources. Grey shade and red lines are normalized kernel density estimation (KDE) plots and probability density plots (PDP), respectively. (A) Combined northern TD samples (Zhang et al., 2016). (B) A mixture of XYH, NYH, ZMH, Bedrock1, Bedrock2, and Bedrock3. (C) Combined southern TD samples excluding TG05 (Zhang et al., 2016). (D) Late Pleistocene WEDP01 samples (~0.05 Ma). (E) Middle Pleistocene WEDP01 samples (~0.87 Ma). (F) XYH sample. (G) NYH sample. (H) ZMH sample. (I) Bedrock1. (J) Bedrock2. (K) Bedrock3.

River sediments and the Northern Tibetan Plateau (NTP) in MDS space. The northern TD, composed of samples TG65, TG15, TG25, TG40, and TG53, plots closer to the Gobi Altay Mountains (GAMs) and Bedrock1 and Bedrock2 (BD1 and BD2), which are similar to each other (Figs. 2 and 3). The drill core samples, H70 and H200, both plot near the southern TD in MDS space. Given the location of the WEDP01 within the TD, this ostensibly suggests that this provenance distribution pattern may have persisted since at least ~ 0.87 Ma, around the time when the desert initially formed.

Sample TG05 from Zhang et al. (2016) is an outlier by location. Although located in the southern TD, its statistically closest neighbor is TG65, a sample located in the northern TD whose statistically closest neighbor is TG15 of the northern region. Sample TG05 may be an outlier due to its proximity to the Yellow River (Fig. 1)—suggesting the Yellow River may have provided sediment to this location. However, the comparison with the upper Yellow River samples does not support this scenario (Fig. 3). Alternatively, this outlier may be the result of a small number of observations (small-*n*), which are often not representative of

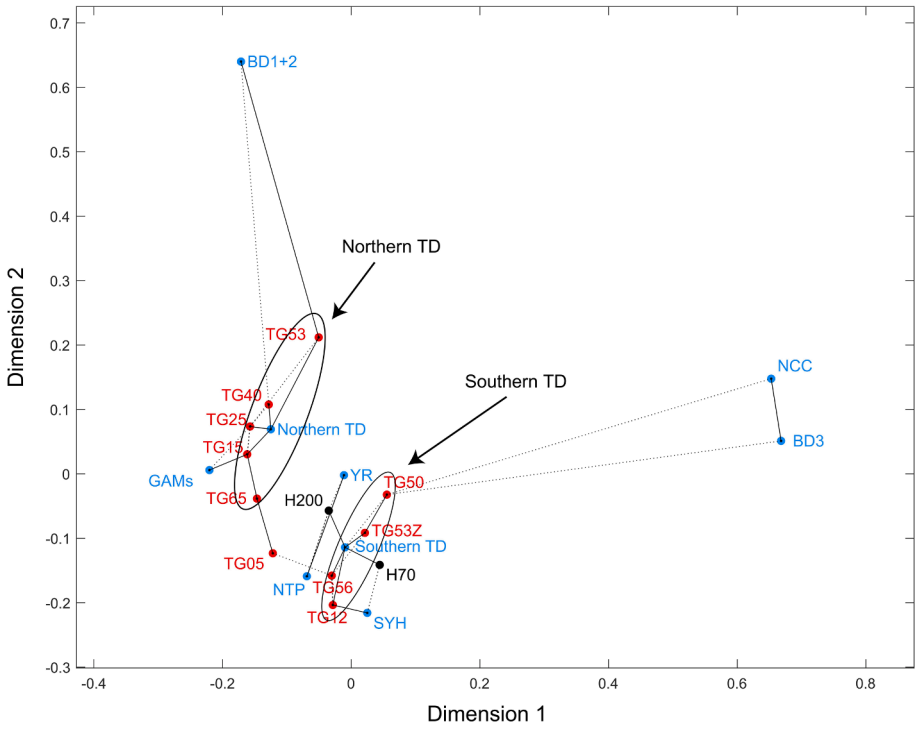

Fig. 3. Non-metric multidimensional scaling (MDS) plot of zircon U-Pb age data from the Tengger Desert (TD) and potential sources. Blue dots represent potential sources and synthesized northern and southern TD samples. Red and black dots represent the TD surface and core WEDP01 samples. Solid and dashed lines mark the closest and second-closest neighbors, respectively. BD3—Bedrock3 sample; BD1 + 2—Bedrock1 and Bedrock2 samples; SYR—XYH, NYH, and ZMH samples; H70—core WEDP01 samples at ~ 0.05 Ma; H200—core WEDP01 samples at ~ 0.87 Ma; GAMs — the Gobi Altay Mountains (Fan et al., 2019); NTP — the Northern Tibetan Plateau (Fan et al., 2019); NCC — North China Craton (Zhang et al., 2016); YR—upper Yellow River (samples 1–8 in Nie et al., 2015).

the 'true' distribution of ages within a sample (Pullen et al., 2014), although major age modes are typically observed (Vermeesch, 2004). Because of this possibility, we exclude TG05 in the following discussion.

To improve the statistical robustness for data comparisons, we combined TG12, TG56, TG53Z, and TG50 to represent the southern TD and combined TG65, TG15, TG25, TG40, and TG53 to represent the northern TD (Figs. 2, 3, 4, 5, 6, and 7). The synthesized southern TD and two drill core samples are distinguished from the synthesized northern TD sample by more ages of 2800–1600 Ma, 1200–800 Ma, and 500–400 Ma, which are also prominent in the three branch river samples of the Shiyang River (Fig. 2), consistent with the pattern in the MDS plot (Fig. 3). By comparison, the northern TD sample is characterized by more 300–200 Ma ages (Fig. 2).

To test different sediment mixing hypotheses for the TD, we apply the inverse Monte Carlo modeling approach of Sundell and Saylor (2017) to the detrital zircon U-Pb ages of these two (combined) synthetic TD samples based on Kolmogorov-Smirnov (KS) test D statistics, Kuiper test V statistics, and cross-correlation coefficient (R) comparison. A total of 30,000 iterations of fitting were applied to assess specific detrital zircon age spectrum by altering the contributions of the potential sources to match the detrital zircon U-Pb cumulative probability curves or probability density plots of the TD samples (Figs. 4 and 6). Data from the TD were compared to U-Pb ages for the combined Shiyang River, Bedrock 1 + 2, Bedrock 3, GAMs, and North China Craton (NCC) (Fig. 4). The modeling experiments show that the GAMs are the most important source for the northern TD (>50%), followed by Bedrock 1 + 2 (~20% in Fig. 5A and C, ~10% in Fig. 5E), and Shiyang River (<20% in Fig. 5A and C, <10% in Fig. 5E). For the southern TD, the GAMs became the second most important source (~30% in Fig. 5B and D), and the most important source is the Shiyang River, accounting for ~ 50% in Fig. 5B and D. In Fig. 5F, however, the GAMs are still the most dominant source for the southern TD, followed by the Shiyang River. Contributions from the NCC and Bedrock 3 are minor (<10%) for the northern TD, and contributions from the NCC and bedrock samples are minor (<10%) for the southern TD.

To test a scenario that considers only proximal sediment sources (i.e., Shiyang River, Bedrock 1 + 2, Bedrock 3) of TD sediments, we did additional modeling which excludes the two distal sources (i.e., GAMs and NCC; Fig. 6). In this scenario, the Shiyang River is the most important source for the northern TD (>50%), followed by Bedrock 1 + 2 (~40% in Fig. 7A, ~30% in Fig. 7C, and ~ 20% in Fig. 7E), and Bedrock 3 (~10% in Fig. 7A, C and E). For the southern TD, the Shiyang River source contributes ~ 70% (Fig. 7B, D, and F), followed by Bedrock 1 + 2 (~15% in Fig. 7B and D, ~20% in Fig. 7F) and Bedrock 3 (<10% in Fig. 7B, D and F).

4. Discussion

Sundell and Saylor (2017) recommend interpreting the modeling results within a geological context, which we will do next. Despite the modeling results suggesting that the GAMs are the most or second most important source for the TD sediments, we suspect that the contribution may not be as high as the modeling suggests. For sand-sized particles to be transported from the GAMs to the TD, the particles would have had to saltate over the Yabulai Mountains (Fig. 1C)—which is within the range of possibilities—or follow an extremely circuitous route that would not align with present-day or middle to late Pleistocene prevailing wind patterns (Fig. 1). The topographic obstacle of the Yabulai Mountains diminishes the eolian transport capacity of the GAMs to the TD sediment pathway. Alternatively, erosion of local bedrock within the TD area is a much more efficient way to produce and transport sediment to the central TD. Similarly, bedrock erosion has been implicated as the dominant sand source in the east Mu Us Desert over a similar interval (Stevens et al., 2013). Indeed, the models excluding the GAMs as a source also yield reasonable results (Figs. 6 and 7), with the Shiyang River as the most dominant source and Bedrock 1 + 2 being a more important source for the northern than southern TD. This is because the main zircon U-Pb age groups from the GAMs source are also shared by the Shiyang River and bedrock samples. For example, although the TD samples have more ages in the range of 400–500 Ma than 200–300 Ma—different from the pattern of the Shiyang River samples—mixing with Bedrock 1 + 2 modifies the pattern to be similar to those of the TD samples. Comparison of the modeling results with or without the GAMs contribution did suggest that the northern TD may have had a

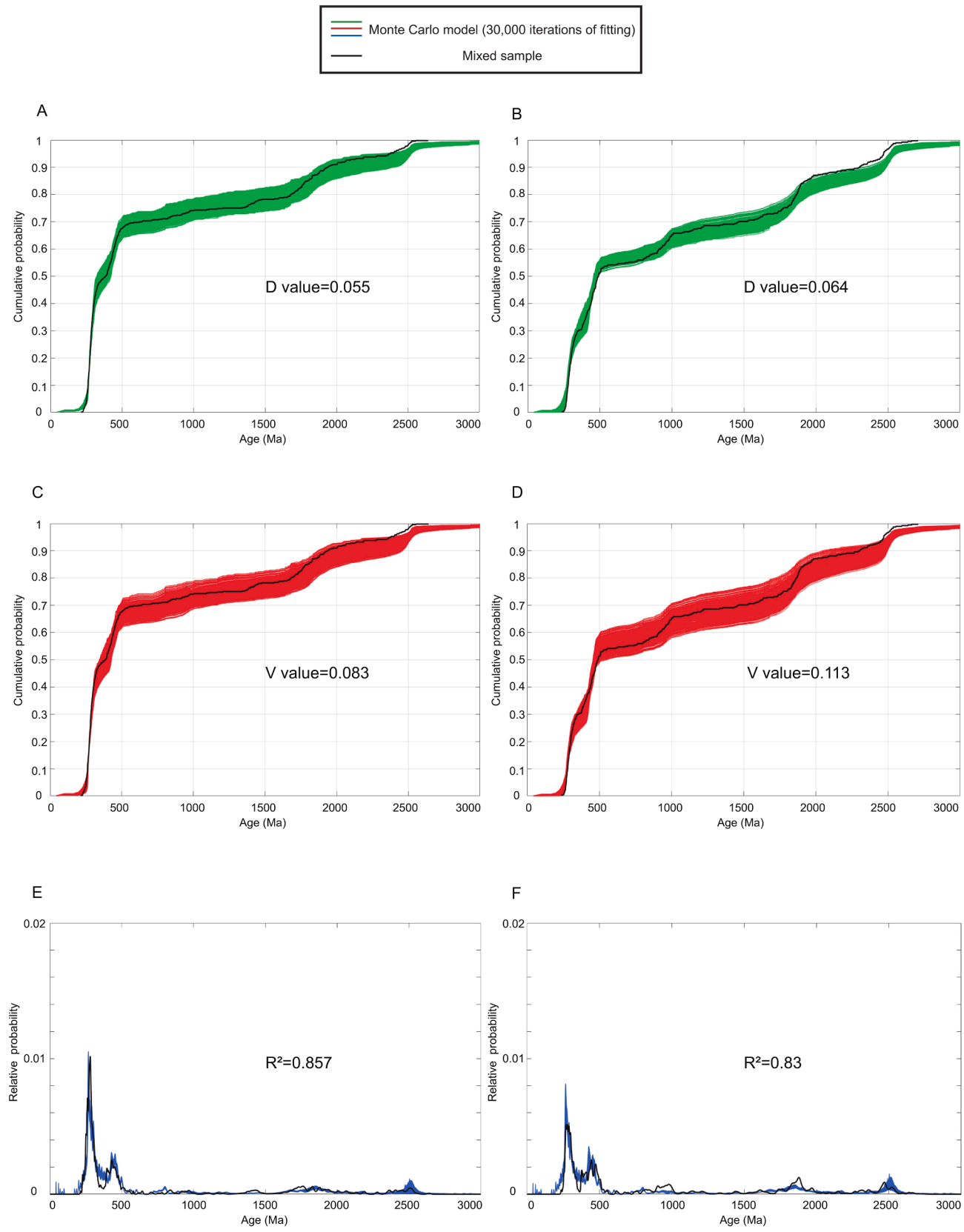

Fig. 4. Model results using the KS test D statistic (A, B), Kuiper test V statistic (C, D), and Cross-correlation coefficient of probability density (E, F) for the TD (northern and southern respectively) zircon U-Pb ages based on SYR, bedrock, GAMs, and NCC. SYR — Combined data of XYH, NYH, and ZMH. GAMs —Gobi Altay Mountains (Fan et al., 2019). NCC — North China Craton (Zhang et al., 2016).

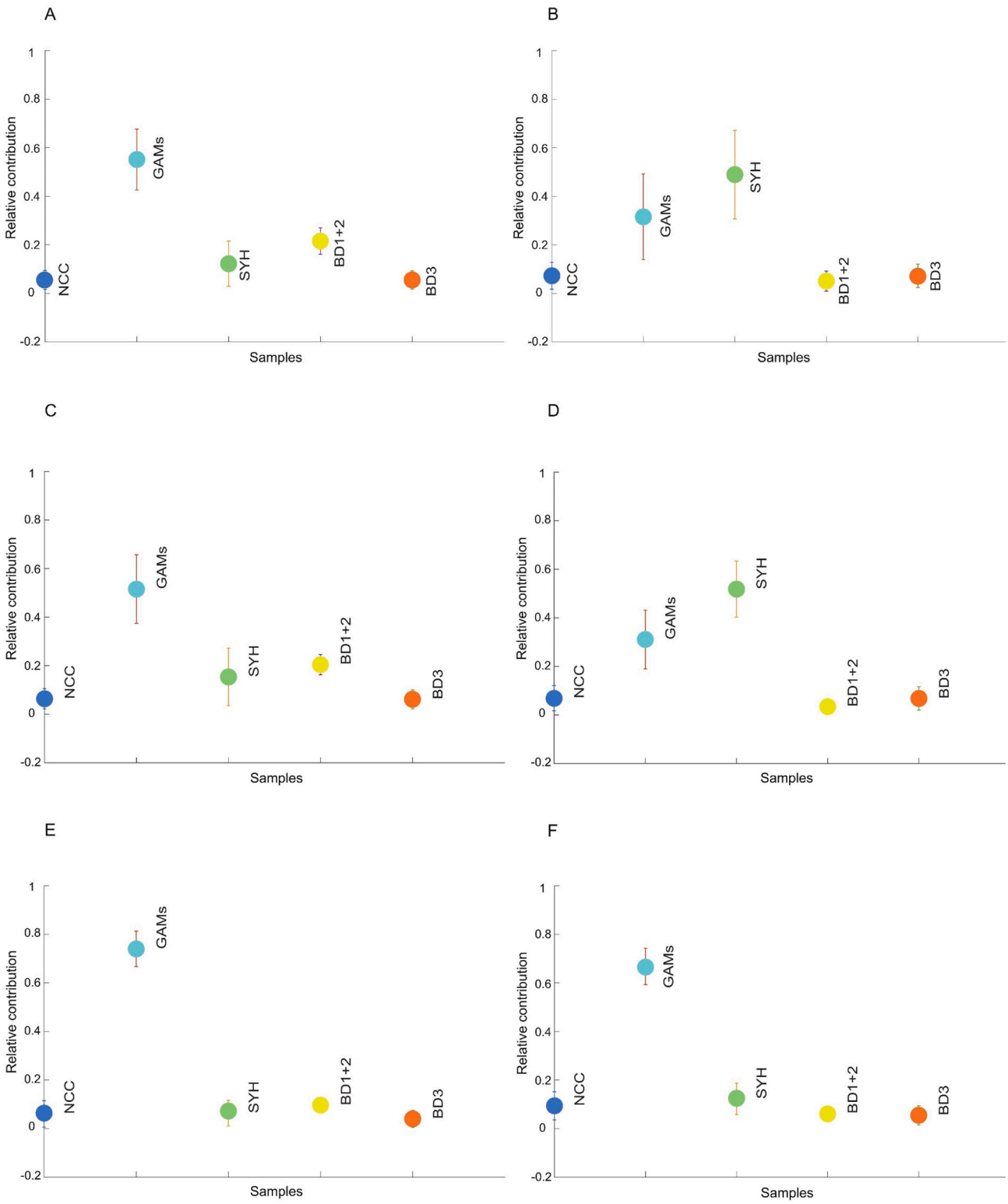

Fig. 5. The relative contribution of the KS test D statistic (A, B), Kuiper test V statistic (C, D), and Cross-correlation coefficient of probability density (E, F) for the TD (northern and southern respectively). SYR — Combined data of XYH, NYH, and ZMH. BD1 + 2 — Combined data of Bedrock1 and Bedrock2. BD3 — Bedrock3. GAMs — the Gobi Altay Mountains (Fan et al., 2019). NCC — North China Craton (Zhang et al., 2016).

contribution from GAMs because the inclusion of the GAMs data can improve the model fitting. This is different from the southern TD data wherein the inclusion of the GAMs contribution did not improve the fitting in a significant way (Fig. 6B and D).

The provenance of the TD is similar to the Mu Us desert in several ways. First, both deserts can be divided into two regions. Zircon U-Pb geochronology, heavy mineral compositions, and trace and rare Earth element data suggest that the Mu Us desert can be divided into a southeastern and a northwestern zone (Stevens et al., 2013; Nie et al., 2015; Ding et al., 2021). The TD can be divided into a northern and a southern zone (Zhang et al., 2016). Second, both have riverine sediments and local basement rocks as important sediment sources.

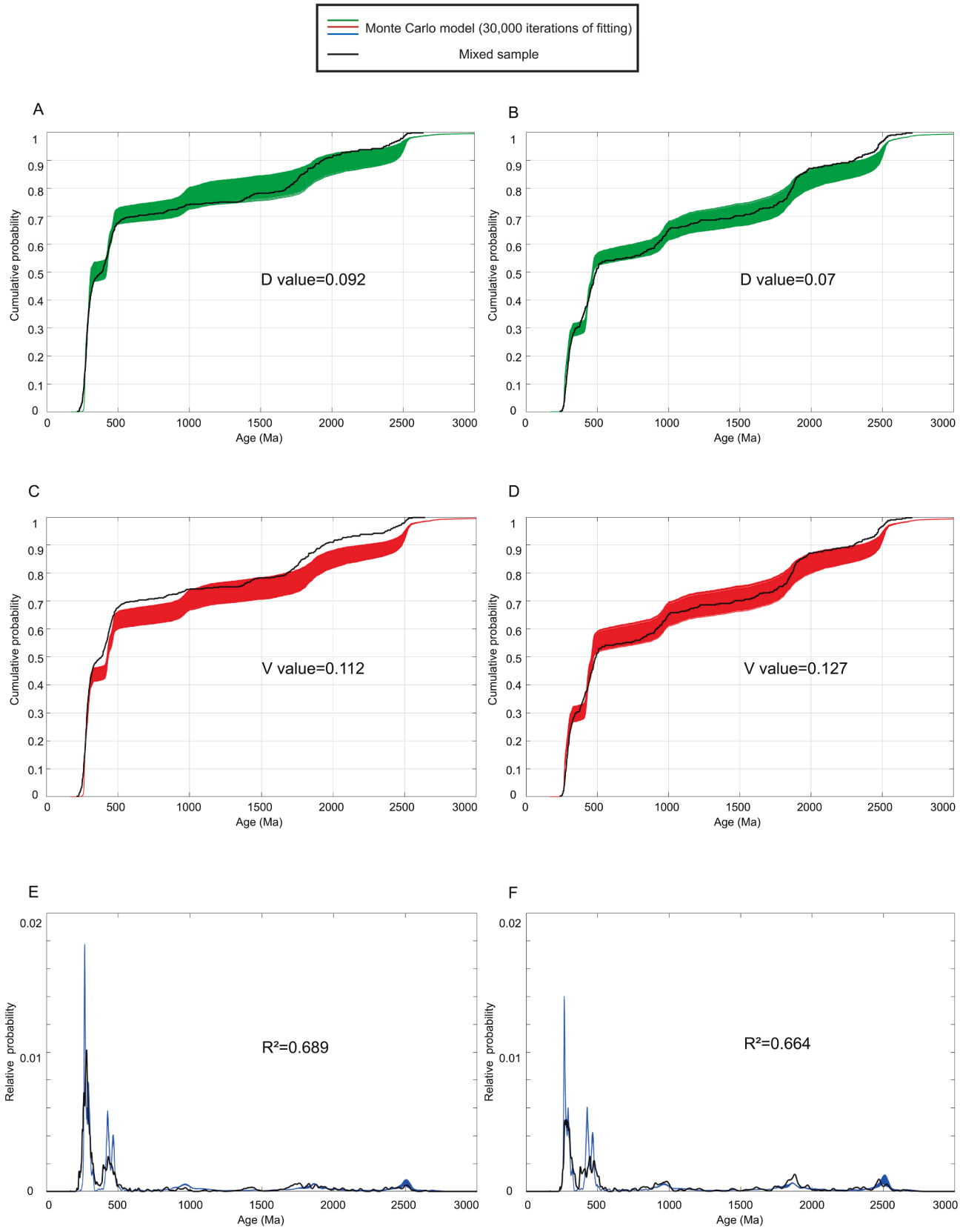

Fig. 6. Model results using the KS test D statistic (A, B), Kuiper test V statistic (C, D), and Cross-correlation coefficient of probability density (E, F) for the TD (northern and southern respectively) zircon U-Pb ages based on SYR and bedrock. SYR — Combined data of XYH, NYH, and ZMH.

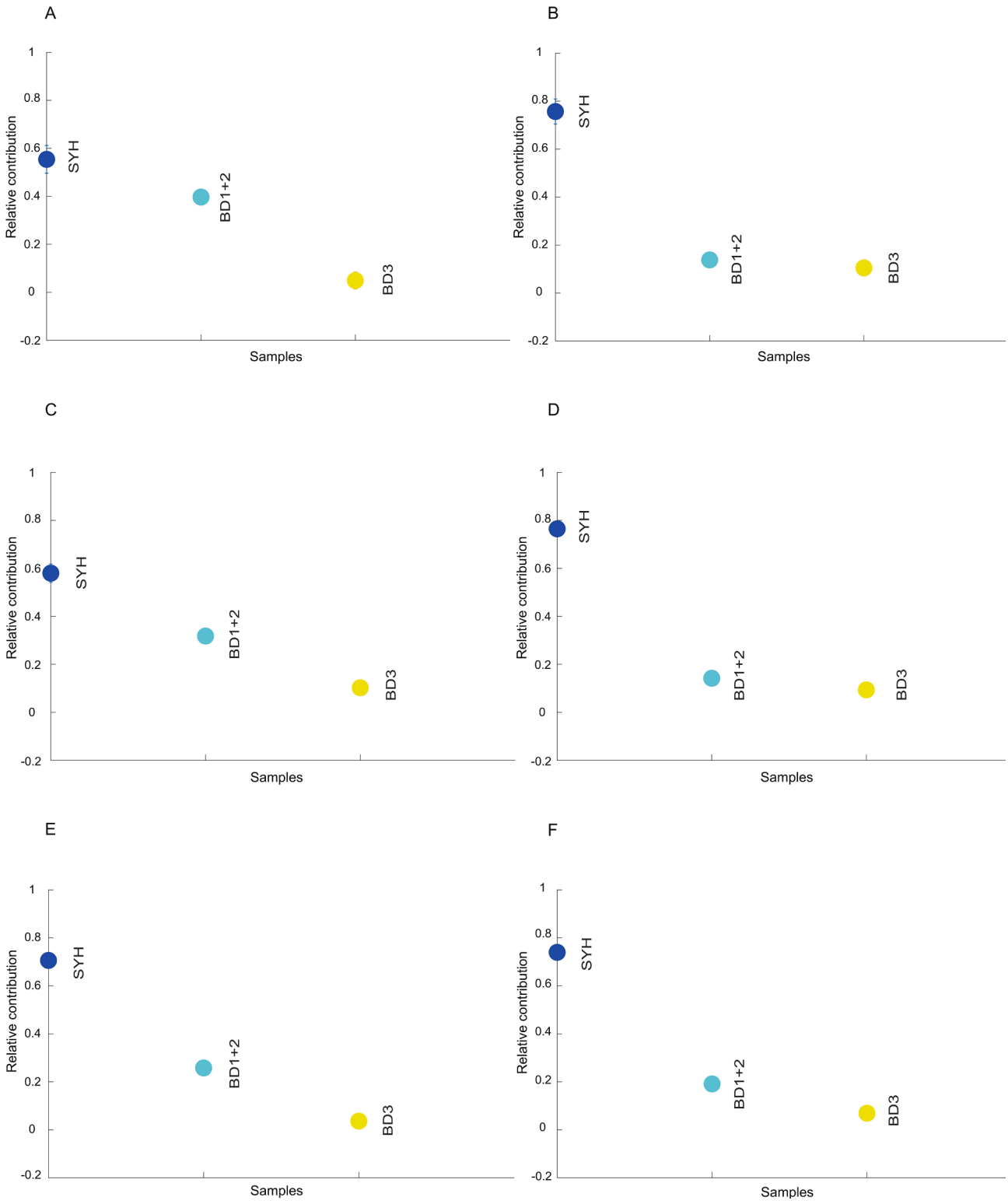

Fig. 7. The relative contribution of the KS test D statistic (A, B), Kuiper test V statistic (C, D), and Cross-correlation coefficient of probability density (E, F) for the TD (northern and southern respectively). SYR — Combined data of XYH, NYH, and ZMH. BD1 + 2 —combined data of Bedrock1 and Bedrock2. BD3 — Bedrock3.

Sediments from the southwestern portion of the Mu Us desert share similar geochemical features with the upper Yellow River sediments bounding the desert to the west. In contrast, sediments from the northeastern portion of the Mu Us desert share similar geochemical features with the exposed basement rocks. Similarly, the Shiyang River, bounding the TD to the southeast, provided a large volume of sediment to its southern zone; in contrast, Bedrock 1 and 2 served as important sources for the northern area of this desert. These findings suggest that there is a common formation pattern for monsoon margin deserts in China: riverine sediment input and local basement erosion.

The fluvial-local bedrock sourcing proposed here for the middle Pleistocene to present TD is consistent with the fluvial-eolian interaction theory for desert formation proposed by Kocurek and Lancaster (1999). This model of desert formation has been applied to the Taklimakan and

the eastern Mu Us Deserts in China (Nie et al., 2015; Yang et al., 2021b). Although potentially coincidental, and thus not an indicator of this model, the formation age of the TD overlaps with the formation age of the Shiyang River (Pan et al., 2003), emphasizing the potential importance of fluvial erosion and transport in desert formation. A sediment core from the south-central Badain Jaran Desert (WEDP02) indicates that the modern eolian landscape formed at ~ 1.1 Ma (Wang et al., 2015). Like the TD, desertification marked a transition away from alluvial and fluvial deposition to eolian, however, some lacustrine deposition persisted. Wang et al. (2015) proposed that the upper Pleistocene eolian sediments were primarily sourced from the Heihe River, originating in the Qilian Mountains, and transported to the basin by westerly-northwesterly winds. Comparing the proposed sourcing of the Badain Jaran and Mu Us sediments with our data for the TD, we find that the middle Pleistocene to present-day sediments of these three monsoon margin deserts share a similar provenance pattern.

Our finding clarifies the surficial processes responsible for dust production and transportation in East Asian deserts located on the margins of the monsoon's influence. It has long been thought that the uplift of the Tibetan Plateau was the primary (and sometimes sole) forcing for desertification in China, either through blocking moisture, preventing vegetation growth which leads to land surface stabilization, or a combination thereof. The data presented here demonstrate that such a scenario would be oversimplified. Different lines of geological evidence demonstrate the present-day Tibetan Plateau likely reached its current configuration in the late Miocene (Zheng et al., 2006; Nie et al., 2019; Ding et al., 2022), with limited subsequent outward growth (Clark et al., 2010; Cheng et al., 2022). If Tibetan uplift and associated moisture blocking are the main reason for Asian desertification, all deserts should have formed at roughly the same time, and no later than the late Miocene. However, that is not consistent with evidences for the middle and late Pleistocene formation of several monsoon margin deserts in northern China (Li et al., 2014b; Wang et al., 2015; Fan et al., 2018). Instead, we suggest that increased wet-dry amplitude variations due to increased glacial-interglacial global temperature and ice volume fluctuations since the middle Pleistocene are important factors in the formation of these monsoon margin deserts in China. These processes increased glacial-related physical weathering and river incision, releasing more unconsolidated sediment and satisfying the sediment supply requirement for desert formation. Increased climatic fluctuation may have also increased frost weathering of exposed basement rocks, producing additional sediment from local sources. Therefore, monsoon marginal deserts may have formed as a result of both increased sediment supply and increased sediment availability, instead of only an aridification-caused sediment availability increase.

Many studies link desert formation primarily to decreasing precipitation often controlled by synoptic climate processes (Sun et al., 2009; Li et al., 2014b). However, the provenance of middle Pleistocene and Holocene sediments in the TD requires precipitation in the sediment transport pathway, even during the proposed increasing aridity in the low-elevation basins. Additionally, because TD desertification occurred around the Mid-Pleistocene Transition, this implies that said desert formation is potentially associated with a greater amplitude of wet-dry and warm-cold cycles, which is known to have increased landscape erosion and sediment accumulation rates elsewhere (Molnar and England, 1990; Medina-Elizalde and Lea, 2005; Elderfield et al., 2012; Sun et al., 2019; Yang et al., 2021a). We speculate that this increased variability of hydroclimate conditions resulted in the release of more detritus from the Qilian Mountains (with glacial processes possibly playing a role) which may have been of similar importance to overall aridification in forcing desertification of the Tengger and Badain Jaran Deserts (Zhao et al., 2022).

We elaborate on the proposed desertification process here. Once more voluminous unconsolidated sediments were supplied by the Qilian Mountains to the TD during the Mid-Pleistocene Transition, and a critical level of aridity was reached in the TD—deflation and eolian transport would have resulted in more aerosol production in the TD. We posit that the elevated aerosol emissions and subsequent atmospheric concentrations—possibly reaching a tipping point in aerosol production—would have produced important local climate feedback effects enhancing the desertification process in the TD. Specifically, increased local atmospheric dust concentrations would promote surface drying by altering the hydrologic cycle. This effect could occur either through *i*) reducing incoming solar radiation and cooling the surface, decreasing convection in the lower atmosphere (Alizadeh Choobari et al., 2012; Huang et al., 2014), *ii*) increasing the number of cloud-condensation nuclei and in turn, small droplets, leading to a reduction in local precipitation (Rosenfeld et al., 2001; Min et al., 2009), or *iii*) enhancing cloud albedo, driving longer rainout periods which typically results in local drying (Teller and Levin, 2006).

5. Conclusions

We hypothesize that more unconsolidated sediments arriving from the Qilian Mountains—driven by East Asian summer monsoon precipitation and stream integration—enhanced desertification of the TD through atmospheric aerosol effects on the local hydroclimate. If valid, this scenario conveys the importance of precipitation on aerosol production and desertification processes (e.g., Huang et al., 2014; Bruner et al., 2022; Zhang et al., 2022). By at least ~ 0.9 Ma the Badain Jaran, Tengger, and Mu Us Deserts were also receiving eolian sediment sourced through rivers draining the Qilian Mountains and northeastern Tibetan Plateau rather than only importing large volumes of sediment from upwind in the more arid continental interior. The association with river transport and the temporal overlap with a key climatic transition of the Pleistocene implies the characteristics of precipitation (i.e., total amount and amplitude of wet-dry cycles) influencing the Qilian Mountains and northern Tibet, along with subsequent dust emission and its localized effects, were critically important in the desertification process of the TD during at least the middle and late Pleistocene.

Declaration of Competing Interest

The authors declare that they have no known competing financial interests or personal relationships that could have appeared to influence the work reported in this paper.

Data availability

Data will be made available on request.

Acknowledgments

We thank two reviewers for constructive comments and Joel Saylor and Kurt Sundell for helpful discussion. This work was financially supported by the National Natural Science Foundation of China (grants 42030505 and 41888101) and the U.S. National Science Foundation (NSF-PIRE #1545859). J. T. A. is currently supported by the U.S. National Science Foundation (NSF-OCE-PRF #2126500).

Appendix A. Supplementary material

Supplementary data to this article can be found online at https://doi.org/10.1016/j.catena.2023.107119.

References

Abell, J.T., Rahimi, S.R., Pullen, A., Lebo, Z.J., Zhang, D., Kapp, P., Gloege, L., Ridge, S., Nie, J., Winckler, G., 2020. A Quantitative Model-Based Assessment of Stony Desert Landscape Evolution in the Hami Basin, China: Implications for Plio-Pleistocene Dust Production in Eastern Asia. Geophys. Res. Lett. 47 e2020GL090064.

Alizadeh Choobari, O., Zawar-Reza, P., Sturman, A., 2012. Feedback between windblown dust and planetary boundary-layer characteristics: Sensitivity to boundary and surface layer parameterizations. Atmos. Environ. 61, 294–304.
An, Z., Kutzbach, J.E., Prell, W.L., Porter, S.C., 2001. Evolution of Asian monsoons and phased uplift of the Himalaya-Tibetan plateau since Late Miocene times. Nature 411, 62–66.
Bovet, P.M., Ritts, B.D., Gehrels, G., Abbink, A.O., Darby, B., Hourigan, J., 2009. Evidence of Miocene crustal shortening in the North Qilian Shan from Cenozoic stratigraphy of the western Hexi Corridor, Gansu Province China. Am. J. Sci. 309, 290.
Bruner, A., Leier, A.L., Barbeau Jr, D.L., Pullen, A., Fidler, M.K., Stubbins, B., 2022. Detrital zircon provenance and transport pathways of Pleistocene-Holocene eolian sediment in the Pampean Plains. Argentina, GSA Bulletin.
Bullard, J.E., Livingstone, I., 2002. Interactions between aeolian and fluvial systems in dryland environments. Area 34, 8–16.
Cheng, F., Garzione, C., Li, X., Salzmann, U., Schwarz, F., Haywood, A.M., Tindall, J., Nie, J., Li, L., Wang, L., Abbott, B.W., Elliott, B., Liu, W., Upadhyay, D., Arnold, A., Tripati, A., 2022. Alpine permafrost could account for a quarter of thawed carbon based on Plio-Pleistocene paleoclimate analogue. Nat. Commun. 13, 1329.
Clark, M.K., Farley, K.A., Zheng, D., Wang, Z., Duvall, A.R., 2010. Early Cenozoic faulting of the northern Tibetan Plateau margin from apatite (U–Th)/He ages. Earth Planet. Sci. Lett. 296, 78–88.
Craddock, W.H., Kirby, E., Harkins, N.W., Zhang, H., Shi, X., Liu, J., 2010. Rapid fluvial incision along the Yellow River during headward basin integration. Nat. Geosci. 3, 209–213.
Ding, Z.L., Derbyshire, E., Yang, S.L., Sun, J.M., Liu, T.S., 2005. Stepwise expansion of desert environment across northern China in the past 3.5 Ma and implications for monsoon evolution. Earth Planet. Sci. Lett. 237, 45–55.
Ding, L., Kapp, P., Cai, F., Garzione, C.N., Xiong, Z., Wang, H., Wang, C., 2022. Timing and mechanisms of Tibetan Plateau uplift. Nat. Rev. Earth Environm. 3, 652–667.
Ding, J., Wu, Y., Tan, L., Fu, T., Du, S., Wen, Y., Li, D., 2021. Trace and rare earth element evidence for the provenances of aeolian sands in the Mu Us Desert NW China. Aeolian Res. 50, 100683.
Duvall, A.R., Clark, M.K., Kirby, E., Farley, K.A., Craddock, W.H., Li, C., Yuan, D.-Y., 2013. Low-temperature thermochronometry along the Kunlun and Haiyuan Faults, NE Tibetan Plateau: Evidence for kinematic change during late-stage orogenesis. Tectonics 32, 1190–1211.
Elderfield, H., Ferretti, P., Greaves, M., Crowhurst, S., McCave, I.N., Hodell, D., Piotrowski, A.M., 2012. Evolution of Ocean Temperature and Ice Volume Through the Mid-Pleistocene Climate Transition. Science 337, 704–709.
Engelstaedter, S., Washington, R., 2007. Temporal controls on global dust emissions: The role of surface gustiness. Geophys. Res. Lett. 34.
Fan, Y., Mou, X., Wang, Y., Liu, C., Zhao, H., Wang, F., Li, Z., Mao, X., Liu, W., Ma, J., Liu, C., Zhang, F., Zhang, F., 2018. Quaternary paleoenvironmental evolution of the Tengger Desert and its implications for the provenance of the loess of the Chinese Loess Plateau. Quat. Sci. Rev. 197, 21–34.
Fan, Y., Li, Z., Wang, F., Ma, J., Mou, X., Li, X., Zhang, Q., Zhao, H., Chen, F., 2019. Provenance variations of the Tengger Desert since 2.35 Ma and its linkage with the Northern Tibetan Plateau: Evidence from U-Pb age spectra of detrital zircons. Quat. Sci. Rev. 223, 105916.
Fang, X., Yan, M., Van der Voo, R., Rea, D.K., Song, C., Parés, J.M., Gao, J., Nie, J., Dai, S., 2005. Late Cenozoic deformation and uplift of the NE Tibetan Plateau: Evidence from high-resolution magnetostratigraphy of the Guide Basin, Qinghai Province, China. GSA Bull. 117, 1208–1225.
Fedorov, A.V., Dekens, P.S., McCarthy, M., Ravelo, A.C., deMenocal, P.B., Barreiro, M., Pacanowski, R.C., Philander, S.G., 2006. The Pliocene Paradox (Mechanisms for a Permanent El Niño). Science 312, 1485–1489.
Garzanti, E., Pastore, G., Stone, A., Vainer, S., Vermeesch, P., Resentini, A., 2022. Provenance of Kalahari Sand: Paleoweathering and recycling in a linked fluvial-aeolian system. Earth Sci. Rev. 224, 103867.
Geng, H., Pan, B., Huang, B., Cao, B., Gao, H., 2017. The spatial distribution of precipitation and topography in the Qilian Shan Mountains, northeastern Tibetan Plateau. Geomorphology 297, 43–54.
George, A.D., Marshallsea, S.J., Wyrwoll, K.-H., Jie, C., Yanchou, L., 2001. Miocene cooling in the northern Qilian Shan, northeastern margin of the Tibetan Plateau, revealed by apatite fission-track and vitrinite-reflectance analysis. Geology 29, 939–942.
Guo, Z.T., Peng, S.Z., Hao, Q.Z., Biscaye, P.E., Liu, T.S., 2001. Origin of the Miocene-Pliocene Red-Earth Formation at Xifeng in Northern China and implications for paleoenvironments. Palaeogeogr. Palaeoclimatol. Palaeoecol. 170, 11–26.
Guo, Z.T., Ruddiman, W.F., Hao, Q.Z., Wu, H.B., Qiao, Y.S., Zhu, R.X., Peng, S.Z., Wei, J. J., Yuan, B.Y., Liu, T.S., 2002. Onset of Asian desertification by 22 Myr ago inferred from loess deposits in China. Nature 416, 159–163.
Haug, G.H., Ganopolski, A., Sigman, D.M., Rosell-Mele, A., Swann, G.E.A., Tiedemann, R., Jaccard, S.L., Bollmann, J., Maslin, M.A., Leng, M.J., Eglinton, G., 2005. North Pacific seasonality and the glaciation of North America 2.7 million years ago. Nature 433, 821–825.
Heermance, R.V., Pearson, J., Moe, A., Langtao, L., Jianhong, X., Jie, C., Richter, F., Garzione, C.N., Junsheng, N., Bogue, S., 2018. Erg deposition and development of the ancestral Taklimakan Desert (western China) between 12.2 and 7.0 Ma. Geology 46, 919–922.
Herbert, T.D., Lawrence, K.T., Tzanova, A., Peterson, L.C., Caballero-Gill, R., Kelly, C.S., 2016. Late Miocene global cooling and the rise of modern ecosystems. Nat. Geosci. 9, 843–847.
Hough, B.G., Garzione, C.N., Wang, Z., Lease, R.O., Burbank, D.W., Yuan, D., 2011. Stable isotope evidence for topographic growth and basin segmentation: Implications for the evolution of the NE Tibetan Plateau. GSA Bull. 123, 168–185.
Huang, J., Wang, T., Wang, W., Li, Z., Yan, H., 2014. Climate effects of dust aerosols over East Asian arid and semiarid regions. J. Geophys. Res. Atmos. 119, 11398–11416.
Kocurek, G., Ewing, R.C., 2005. Aeolian dune field self-organization – implications for the formation of simple versus complex dune-field patterns. Geomorphology 72, 94–105.
Kocurek, G., Lancaster, N., 1999. Aeolian system sediment state: theory and Mojave Desert Kelso dune field example. Sedimentology 46, 505–515.
Kok, J.F., Adebiyi, A.A., Albani, S., Balkanski, Y., Checa-Garcia, R., Chin, M., Colarco, P. R., Hamilton, D.S., Huang, Y., Ito, A., Klose, M., Leung, D.M., Li, L., Mahowald, N.M., Miller, R.L., Obiso, V., Pérez García-Pando, C., Rocha-Lima, A., Wan, J.S., Whicker, C.A., 2021. Improved representation of the global dust cycle using observational constraints on dust properties and abundance. Atmos. Chem. Phys. 21, 8127–8167.
Kurosaki, Y., Mikami, M., 2003. Recent frequent dust events and their relation to surface wind in East Asia. Geophysical Research Letters, 30.
Li, J., Fang, X., Song, C., Pan, B., Ma, Y., Yan, M., 2014a. Late Miocene-Quaternary rapid stepwise uplift of the NE Tibetan Plateau and its effects on climatic and environmental changes. Quat. Res. 81, 400–423.
Li, Z., Sun, D., Chen, F., Wang, F., Zhang, Y., Guo, F., Wang, X., Li, B., 2014b. Chronology and paleoenvironmental records of a drill core in the central Tengger Desert of China. Quat. Sci. Rev. 85, 85–98.
Li, Z., Gao, Y., Wang, Y., Pan, Y., Li, J., Chen, A., Wang, T., Han, C., Song, Y., Theakstone, W.H., 2015. Can monsoon moisture arrive in the Qilian Mountains in summer? Quat. Int. 358, 113–125.
Li, Z., Wang, F., Wang, X., Li, B., Chen, F., 2018. A multi-proxy climatic record from the central Tengger Desert, southern Mongolian Plateau: Implications for the aridification of inner Asia since the late Pliocene. J. Asian Earth Sci. 160, 27–37.
Liu, W., Liu, Z., Sun, J., Song, C., Chang, H., Wang, H., Wang, Z., An, Z., 2020. Onset of permanent Taklimakan Desert linked to the mid-Pleistocene transition. Geology 48, 782–786.
Martin, J.H., 1990. Glacial-interglacial CO2 change: The Iron Hypothesis. Paleoceanography 5, 1–13.
McGee, D., Broecker, W.S., Winckler, G., 2010. Gustiness: The driver of glacial dustiness? Quat. Sci. Rev. 29, 2340–2350.
Medina-Elizalde, M., Lea, D.W., 2005. The Mid-Pleistocene Transition in the Tropical Pacific. Science 310, 1009–1012.
Min, Q.L., Li, R., Lin, B., Joseph, E., Wang, S., Hu, Y., Morris, V., Chang, F., 2009. Evidence of mineral dust altering cloud microphysics and precipitation. Atmos. Chem. Phys. 9, 3223–3231, 3223–3231.
Molnar, P., England, P., 1990. Late Cenozoic uplift of mountain ranges and global climate change: chicken or egg? Nature 346, 29–34.
Nie, J., Zhang, R., Necula, C., Heslop, D., Liu, Q., Gong, L., Banerjee, S., 2014. Late Miocene–early Pleistocene paleoclimate history of the Chinese Loess Plateau revealed by remanence unmixing. Geophys. Res. Lett. 41, 2163–2168.
Nie, J., Stevens, T., Rittner, M., Stockli, D., Garzanti, E., Limonta, M., Bird, A., Andò, S., Vermeesch, P., Saylor, J., Lu, H., Breecker, D., Hu, X., Liu, S., Resentini, A., Vezzoli, G., Peng, W., Carter, A., Ji, S., Pan, B., 2015. Loess Plateau storage of Northeastern Tibetan Plateau-derived Yellow River sediment. Nat. Commun. 6, 8511.
Nie, J., Ren, X., Saylor, J.E., Su, Q., Horton, B.K., Bush, M.A., Chen, W., Pfaff, K., 2019. Magnetic polarity stratigraphy, provenance, and paleoclimate analysis of Cenozoic strata in the Qaidam Basin, NE Tibetan Plateau. GSA Bull. 132, 310–320.
Pan, B., Burbank, D., Wang, Y., Wu, G., Li, J., Guan, Q., 2003. A 900 k.y. record of strath terrace formation during glacial-interglacial transitions in northwest China. Geology 31, 957–960.
Pastore, G., Baird, T., Vermeesch, P., Bristow, C., Resentini, A., Garzanti, E., 2021. Provenance and recycling of Sahara Desert sand. Earth Sci. Rev. 216, 103606.
Pullen, A., Kapp, P., McCallister, A.T., Chang, H., Gehrels, G.E., Garzione, C.N., Heermance, R.V., Ding, L., 2011. Qaidam Basin and northern Tibetan Plateau as dust sources for the Chinese Loess Plateau and paleoclimatic implications. Geology 39, 1031–1034.
Pullen, A., Ibáñez-Mejía, M., Gehrels, G.E., Ibáñez-Mejía, J.C., Pecha, M., 2014. What happens when n= 1000? Creating large-n geochronological datasets with LA-ICP-MS for geologic investigations. J. Anal. At. Spectrom 29, 971–980.
Qiang, X.K., Li, Z.X., Powell, C.M., Zheng, H.B., 2001. Magnetostratigraphic record of the Late Miocene onset of the East Asian monsoon, and Pliocene uplift of northern Tibet. Earth Planet. Sci. Lett. 187, 83–93.
Ravelo, A.C., Andreasen, D.H., Lyle, M., Olivarez Lyle, A., Wara, M.W., 2004. Regional climate shifts caused by gradual global cooling in the Pliocene epoch. Nature 429, 263–267.
Raymo, M.E., Lisiecki, L.E., Nisancioglu Kerim, H., 2006. Plio-Pleistocene Ice Volume, Antarctic Climate, and the Global δ18O Record. Science 313, 492–495.
Rittner, M., Vermeesch, P., Carter, A., Bird, A., Stevens, T., Garzanti, E., Andò, S., Vezzoli, G., Dutt, R., Xu, Z., Lu, H., 2016. The provenance of Taklamakan desert sand. Earth Planet. Sci. Lett. 437, 127–137.
Roe, G., 2009. On the interpretation of Chinese loess as a paleoclimate indicator. Quat. Res. 71, 150–161.
Rosenfeld, D., Rudich, Y., Lahav, R., 2001. Desert dust suppressing precipitation: A possible desertification feedback loop. Proc. Natl. Acad. Sci. 98, 5975–5980.
Saylor, J.E., Jordan, J.C., Sundell, K.E., Wang, X., Wang, S., Deng, T., 2018. Topographic growth of the Jishi Shan and its impact on basin and hydrology evolution, NE Tibetan Plateau. Basin Res. 30, 544–563.

Song, Y., Fang, X., Li, J., An, Z., Miao, X., 2001. The Late Cenozoic uplift of the Liupan Shan, China. Sci China Ser D Earth Sci 44, 176–184.
Stevens, T., Carter, A., Watson, T.P., Vermeesch, P., Andò, S., Bird, A.F., Lu, H., Garzanti, E., Cottam, M.A., Sevastjanova, I., 2013. Genetic linkage between the Yellow River, the Mu Us desert and the Chinese Loess Plateau. Quat. Sci. Rev. 78, 355–368.
Sun, D., An, Z., Shaw, J., Bloemendal, J., Sun, Y., 1998. Magnetostratigraphy and palaeoclimatic significance of Late Tertiary aeolian sequences in the Chinese Loess Plateau. Geophys. J. Int. 134, 207–212.
Sun, D., Bloemendal, J., Yi, Z., Zhu, Y., Wang, X., Zhang, Y., Li, Z., Wang, F., Han, F., Zhang, Y., 2011. Palaeomagnetic and palaeoenvironmental study of two parallel sections of late Cenozoic strata in the central Taklimakan Desert: Implications for the desertification of the Tarim Basin. Palaeogeogr. Palaeoclimatol. Palaeoecol. 300, 1–10.
Sun, J., Liu, T., 2006. The Age of the Taklimakan Desert. Science 312, 1621-1621.
Sun, Y., Yin, Q., Crucifix, M., Clemens, S.C., Araya-Melo, P., Liu, W., Qiang, X., Liu, Q., Zhao, H., Liang, L., Chen, H., Li, Y., Zhang, L., Dong, G., Li, M., Zhou, W., Berger, A., An, Z., 2019. Diverse manifestations of the mid-Pleistocene climate transition. Nat. Commun. 10, 352.
Sun, J., Zhang, Z., Zhang, L., 2009. New evidence on the age of the Taklimakan Desert. Geology 37, 159–162.
Sun, J., Liu, W., Liu, Z., Deng, T., Windley, B.F., Fu, B., 2017. Extreme aridification since the beginning of the Pliocene in the Tarim Basin, western China. Palaeogeogr. Palaeoclimatol. Palaeoecol. 485, 189–200.
Sundell, K.E., Gehrels, G.E., Pecha, M.E., 2021. Rapid U-Pb Geochronology by Laser Ablation Multi-Collector ICP-MS. Geostand. Geoanal. Res. 45, 37–57.
Sundell, K.E., Saylor, J.E., 2017. Unmixing detrital geochronology age distributions. Geochem. Geophys. Geosyst. 18, 2872–2886.
Tagliabue, A., Bowie, A.R., Boyd, P.W., Buck, K.N., Johnson, K.S., Saito, M.A., 2017. The integral role of iron in ocean biogeochemistry. Nature 543, 51–59.
Teller, A., Levin, Z., 2006. The effects of aerosols on precipitation and dimensions of subtropical clouds: a sensitivity study using a numerical cloud model. Atmos. Chem. Phys. 6, 67–80, 67–80.
Újvári, G., Klötzli, U., Stevens, T., Svensson, A., Ludwig, P., Vennemann, T., Gier, S., Horschinegg, M., Palcsu, L., Hippler, D., Kovács, J., Di Biagio, C., Formenti, P., 2022. Greenland ice core record of last glacial dust sources and atmospheric circulation. J. Geophys. Res. Atmospheres n/a, e2022JD036597.
Uno, I., Eguchi, K., Yumimoto, K., Takemura, T., Shimizu, A., Uematsu, M., Liu, Z., Wang, Z., Hara, Y., Sugimoto, N., 2009. Asian dust transported one full circuit around the globe. Nat. Geosci. 2, 557–560.
Vermeesch, P., 2004. How many grains are needed for a provenance study? Earth Planet. Sci. Lett. 224, 441–451.
Vermeesch, P., 2013. Multi-sample comparison of detrital age distributions. Chem. Geol. 341, 140–146.
Wang, F., Sun, D., Chen, F., Bloemendal, J., Guo, F., Li, Z., Zhang, Y., Li, B., Wang, X., 2015. Formation and evolution of the Badain Jaran Desert, North China, as revealed by a drill core from the desert centre and by geological survey. Palaeogeogr. Palaeoclimatol. Palaeoecol. 426, 139–158.
Yang, J., Nie, J., Garzanti, E., Limonta, M., Andò, S., Vermeesch, P., Zhang, H., Hu, X., Wang, Z., Zhao, B., Ncube, L., Stevens, T., Li, M., Li, H., Chen, T., Miao, Y., Pan, B., 2021a. Climatic Forcing of Plio-Pleistocene Formation of the Modern Limpopo River, South Africa. Geophys. Res. Lett. 48 e2021GL093887.
Yang, X., Scuderi Louis, A., Wang, X., Scuderi Louis, J., Zhang, D., Li, H., Forman, S., Xu, Q., Wang, R., Huang, W., Yang, S., 2015. Groundwater sapping as the cause of irreversible desertification of Hunshandake Sandy Lands, Inner Mongolia, northern China. Proc. Natl. Acad. Sci. 112, 702–706.
Yang, X., Du, J., Liang, P., Zhang, D., Chen, B., Rioual, P., Zhang, F., Li, H., Wang, X., 2021b. Palaeoenvironmental changes in the central part of the Taklamakan Desert, northwestern China sincethe late Pleistocene. Chin. Sci. Bull. 66, 3205.
Zhang, R., Jiang, D., Zhang, Z., Yu, E., 2015. The impact of regional uplift of the Tibetan Plateau on the Asian monsoon climate. Palaeogeogr. Palaeoclimatol. Palaeoecol. 417, 137–150.
Zhang, H., Lu, H., Xu, X., Liu, X., Yang, T., Stevens, T., Bird, A., Xu, Z., Zhang, T., Lei, F., Feng, H., 2016. Quantitative estimation of the contribution of dust sources to Chinese loess using detrital zircon U-Pb age patterns. J. Geophys. Res. Earth 121, 2085–2099.
Zhang, D., Wang, G., Abell, J.T., Pullen, A., Winckler, G., Schaefer, J.M., Shen, T., 2022. Quantifying Late Pleistocene to Holocene Erosion Rates in the Hami Basin, China: Insights Into Pleistocene Dust Dynamics of an East Asian Stony Desert. Geophys. Res. Lett. 49 e2021GL097495.
Zhao, H., Sun, Y., Qiang, X., 2022. Mid-Pleistocene formation of modern-like desert landscape in North China. Catena 216, 106399.
Zheng, D., Zhang, P.-Z., Wan, J., Yuan, D., Li, C., Yin, G., Zhang, G., Wang, Z., Min, W., Chen, J., 2006. Rapid exhumation at ~8 Ma on the Liupan Shan thrust fault from apatite fission-track thermochronology: Implications for growth of the northeastern Tibetan Plateau margin. Earth Planet. Sci. Lett. 248, 198–208.
Zheng, D., Clark, M.K., Zhang, P., Zheng, W., Farley, K.A., 2010. Erosion, fault initiation and topographic growth of the North Qilian Shan (northern Tibetan Plateau). Geosphere 6, 937–941.
Zheng, H., Wei, X., Tada, R., Clift Peter, D., Wang, B., Jourdan, F., Wang, P., He, M., 2015. Late Oligocene–early Miocene birth of the Taklimakan Desert. Proc. Natl. Acad. Sci. 112, 7662–7667.